MITLibraries | DSpace@MIT

MIT Open Access Articles

First-principles study of the oxygen evolution reaction of lithium peroxide in the lithium-air battery

Massachusetts Institute of Technology

First-principles study of the oxygen evolution reaction of lithium peroxide in the lithium-air battery

Yifei Mo, Shyue Ping Ong, and Gerbrand Ceder[*]

Department of Materials Science and Engineering, Massachusetts Institute of Technology, Cambridge, Massachusetts 02139
(Received 2 September 2011; revised manuscript received 2 November 2011; published 21 November 2011)

The lithium-air chemistry is an interesting candidate for the next-generation batteries with high specific energy. However, this new battery technology is facing substantial challenges, such as a high overpotential upon charging, poor reversibility, and low power density. Using first-principles calculations, we study the oxygen evolution reaction (OER) on the low-index surfaces of lithium peroxide. The elementary reaction steps and the energy profile of the OER are identified on the low-index surfaces of lithium peroxide. We find that the OER processes are kinetically limited by the high energy barrier for the evolution of oxygen molecules and that the rate of the OER processes is highly dependent on the surface orientation.
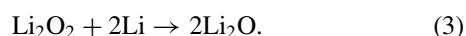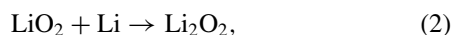
I. INTRODUCTION

To address the demands in energy storage for the next generation of electric vehicles, there is a strong motivation in seeking batteries with higher specific energies and higher energy densities. Metal-air battery systems have the potential to provide significantly higher specific energies than current lithium-ion batteries. In particular, the lithium-air battery system, which was first demonstrated by Abraham and Jiang,[1] has attracted significant interest because of its high theoretical specific energy of up to ~3400 Wh per kg of its electrode materials.

However, there are substantial challenges that Li-air battery technology needs to overcome before widespread commercial adoption is possible. Current Li-air batteries suffer from poor cyclability (up to only tens of cycles) and reversibility.[2–7] They also have low energy efficiencies, with charging voltages as high as 4.0–4.5 V and discharge voltages of about 2.5–3.0 V.[2–6] To improve the rechargeability and energy efficiency of Li-air batteries, catalysts have been used at the air cathode.[2–6,8–10] For example, Pt/Au nanoparticles[9] or Pd/MnO$_2$ catalysts[5,6] help lower the charging voltage to 3.6 V, thereby increasing the cyclic efficiency to ~80%.

Recent studies have also identified that a possible cause of the high-voltage hysteresis is due to side reactions of the electrolyte with the discharge product of the Li-air reaction, Li$_2$O$_2$, which forms lithium carbonate and lithium alkyl carbonates with the carbonate species in the electrolyte.[11–14] These side reactions deplete the electrolyte during cycling and limit the reversibility of Li-air batteries.

The power density of current Li-air batteries is very low with current densities of about 0.1–1 mA/cm^2 (Refs. 1,2,10,15, and 16), which is at least one order of magnitude lower than the requirements for electric vehicle applications.[17] Gaining a better understanding of the fundamental mechanisms of the cathode reactions, such as the oxygen reduction reaction (ORR) during discharge and the oxygen evolution reaction (OER) during charge, is essential to guide the experimental efforts in improving the performance of the Li-air battery. Three elementary reaction steps have been proposed for the ORR:[15,18,19]

$$\text{Li} + \text{O}_2 \rightarrow \text{LiO}_2, \qquad (1)$$

$$\text{LiO}_2 + \text{Li} \rightarrow \text{Li}_2\text{O}_2, \qquad (2)$$

$$\text{Li}_2\text{O}_2 + 2\text{Li} \rightarrow 2\text{Li}_2\text{O}. \qquad (3)$$

Recent *ab initio* modeling has also provided the energy profile and reaction path for the ORR of Li$_2$O$_2$[20] as well as the ORR on catalytic metal surfaces, such as Au and Pt.[21] However, to our knowledge, no similar experimental or theoretical work has yet been performed on the fundamental mechanism of the OER process, such as the elementary reaction steps and the reaction energy profile.

Because the OER process is essentially the decomposition of Li$_2$O$_2$ from its surfaces, the details of the reaction path and desorption barrier will be affected by the surface structure. In this study, we determine from first principles the lowest energy surfaces and the Wulff shape of Li$_2$O$_2$, and the energy barriers for oxygen evolution on the dominant surfaces. We try to provide some insight into whether high overpotential and low charging rate of Li-air batteries are caused by the sluggish kinetics of decomposing Li$_2$O$_2$.

II. METHODS

All total energies were calculated using the generalized gradient approximation (GGA) to density functional theory (DFT). The calculations were performed using the Vienna *ab initio* simulation package (VASP)[22] within the projector augmented-wave (PAW) approach.[23] An energy cutoff of 500 eV for the plane-wave basis set and appropriate k-point meshes were chosen to ensure that the energies were converged within 1 meV per formula unit of lithium peroxide. All structures were fully relaxed.

Surface energy calculations were performed using supercells comprising alternating infinite slabs of Li$_2$O$_2$ with vacuum regions.[24–31] Based on our convergence tests, we found that a vacuum thickness of 10 Å and Li$_2$O$_2$ layer thickness of ~30 Å are sufficient to obtain convergence of the surface energies to within 1 meV/Å^2. These thicknesses were used throughout our simulations, and both surfaces of a Li$_2$O$_2$ slab are kept symmetrically equivalent in all cases.

Using the slab/vacuum supercell model, the surface energy is then given by the following expression:

$$\gamma = \frac{1}{2A}\left(G_{\text{slab}} - N_{\text{Li}} \cdot \mu_{\text{Li}}^{\text{Li}_2\text{O}_2} - N_{\text{O}} \cdot \mu_{\text{O}}^{\text{Li}_2\text{O}_2}\right), \qquad (4)$$

where G_{slab} is the total free energy of the slab/vacuum supercell, A is the area of one surface of the slab, the fraction of 1/2 is to account for the two surfaces in the slab, N_{Li} and

N_O are the number of Li and O atoms, respectively, and $\mu_{Li}^{Li_2O_2}$ and oxygen $\mu_O^{Li_2O_2}$ is the chemical potentials of lithium and oxygen, respectively.

A. Ranges of chemical potentials

The surface energies of nonstoichiometric terminations are affected by the chemical potentials of lithium $\mu_{Li}^{Li_2O_2}$ and oxygen $\mu_O^{Li_2O_2}$. The formalism to determine the allowable range of the chemical potentials has been well established in the literature.[26–28,31–35] In this study, we determine the surface energy in a range of chemical potentials consistent with Li_2O_2 being stable with respect to either Li_2O or oxygen gas under standard conditions (298 K and 1 bar). The maximum chemical potential of Li is defined by the formation of Li_2O from Li_2O_2,

$$\mu_{Li}^{max} = G^{Li_2O} - \tfrac{1}{2}G^{Li_2O_2}, \quad (5)$$
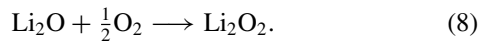
where $G^{Li_2O_2}$ and G^{Li_2O} are the free energy per formula unit of Li_2O_2 and Li_2O. The minimum chemical potential of Li occurs when Li_2O_2 is reduced to release O_2 and can be written as

$$\mu_{Li}^{max} + \Delta G_r < \mu_{Li}^{Li_2O_2}, \quad (6)$$

where

$$\Delta G_r = G^{Li_2O_2} - G^{Li_2O} - \mu_O^0 \quad (7)$$

is the free energy of the following reaction:

$$Li_2O + \tfrac{1}{2}O_2 \longrightarrow Li_2O_2. \quad (8)$$

In Eq. (7), μ_O^0 is the chemical potential of oxygen gas under standard conditions (298 K and 1 bar).

The chemical potentials of Li and O are not independent and are linked by the following expression:

$$\tfrac{1}{2}G^{Li_2O_2} = \mu_{Li}^{Li_2O_2} + \mu_O^{Li_2O_2}. \quad (9)$$

Therefore, the surface energy can be written as the following:

$$\gamma = \frac{1}{2A}\left[G_{slab} - \frac{N_O}{2} \cdot G^{Li_2O_2} - (N_{Li} - N_O) \cdot \mu_{Li}^{Li_2O_2} \right]. \quad (10)$$

N_{Li} and N_O are the number of Li and O atoms in the slab.

The chemical potential range defined in Eqs. (5) and (6) is the most relevant to describe the charging process of Li_2O_2. In discharging, the Li chemical potential could take on higher values. While under equilibrium conditions, the Li chemical potential is bound by its value in the Li_2O_2-Li_2O equilibrium, kinetic limitations in the formation of Li_2O could allow the voltage to drop, and hence $\mu_{Li}^{Li_2O_2}$ to rise above its equilibrium value. For this reason, we also investigated the surfaces of Li_2O_2 under high $\mu_{Li}^{Li_2O_2}$.

Several approximations have to be made to the free energies and chemical potential to turn Eqs. (4)–(10) into a computationally feasible scheme. We assume that the PV and entropy contribution to the free energy of all solid phases (Li_2O_2, Li_2O, Li) are small compared to the entropic contribution in the free energy of gas phases so that the free energy of the solids can be approximated by their zero K energy.

B. The oxygen chemical potential

As can be observed from Eq. (7), the range of chemical potentials is dependent on the chemical potential of O_2 and on the formation energy of Li_2O_2. It has been well established that the standard GGA approximation significantly overestimates the binding energy of the O=O bond in O_2.[36] Wang *et al.*[36] have earlier determined an adjustment of -1.36 eV/molecule for the GGA O_2 energy by fitting the formation energies of Li_2O and other main group oxides. Using the corrected O_2 energy by Wang *et al.*,[36] the formation energy of Li_2O_2 from Li metal and O_2 gas under standard conditions is -6.46 eV per formula, which is significantly lower than the experimental value of -5.93 eV per formula unit. The error in the formation energy of Li_2O_2 is caused by the fact that the relevant reaction (8), that is, $Li_2O + \tfrac{1}{2}O_2 \rightarrow Li_2O_2$, involves oxygen in three different bonding environments and oxidation states, namely, molecular O_2, O^{2-} in Li_2O, and O_2^{2-} in Li_2O_2. It is not possible to determine a single correction to the O_2 GGA energy that would accurately reproduce the experimental formation energies of both Li_2O and Li_2O_2, given that the O=O bond is completely broken in the formation of Li_2O while it is only partially broken in the formation of Li_2O_2. Hence, we have adopted the approach of fitting the O_2 chemical potential to reproduce the reaction free energy ΔG_r. This defines μ_O^0 as

$$\mu_O^0 = E^{Li_2O_2}(GGA) - E^{Li_2O}(GGA) - \Delta G_r(Expt)$$
$$= -4.985 \text{ eV}. \quad (11)$$

Because this value of μ_O^0 is determined from an experimental reaction free energy, it contains oxygen gas entropy as well as any correction to the energy due to GGA errors in $E^{Li_2O_2}$ and E^{Li_2O}. In addition, this value of μ_O^0 can only be used for the chemical potential of oxygen gas under 298 K and 1 bar. To apply at other temperatures, the experimental entropy of O_2 gas at the corresponding condition would have to be used to modify μ_O^0.

III. LOW-INDEX SURFACES OF LITHIUM PEROXIDE

To calculate the surface energy and surface structure, we constructed slab models of the (0001), (11$\bar{2}$0), (1$\bar{1}$00), (11$\bar{2}$1), (1$\bar{1}$01) surfaces. Different terminations were constructed by removing different atoms on the surface.

A. (0001) surface

We considered four terminations for the (0001) surface. These terminations are the O(1)-Li(1)-O(2)-Li(2), Li(1)-O(2)-Li(2), O(2)-Li(2), and Li(2) terminations, which are denoted by the atoms remaining on the surface after removing selected atoms from different sites in the surface unit cell, as labeled in Fig. 1(a). The O(1)-Li(1)-O(2)-Li(2) termination is shown in Fig. 1(a). The other three terminations are generated as follows. The Li(1)-O(2)-Li(2) termination is generated by removing all oxygen atoms from the O(1) site. We construct the O(2)-Li(2) termination from the Li(1)-O(2)-Li(2) termination by removing the Li atoms from Li(1) site. The Li(2) termination is generated by removing atoms from Li(1), O(1), and O(2) sites. All these four terminations are off-stoichiometric. Therefore, the surface energies of these terminations depend on the
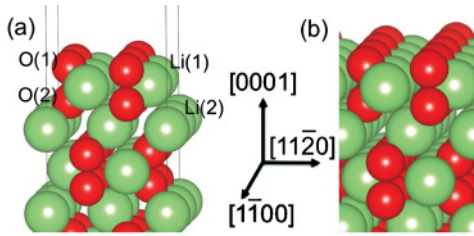
FIG. 1. (Color online) (a) The surface unit cell and (b) the relaxed structure of the most stable termination of the (0001) surface. Red and green atoms are oxygen and lithium, respectively.

chemical potential of both Li and O_2. We considered the surface energy in the range of chemical potentials specified in the Methods section. Our calculations show that the O(1)-Li(1)-O(2)-Li(2) termination shown in Fig. 1(b) is the most stable termination. The study by Seriani[37] predicted the same termination on the (0001) surface to be the most stable. Surfaces terminated by Li atoms, that is, Li(1)-O(2)-Li(2) and Li(2) terminations, are found to be less favorable (see Table II in the Appendix). The O(2)-Li(2) oxygen terminated has considerably higher surface energy. The high surface energy of the O(2)-Li(2) termination is probably due to the breakage of the covalent peroxide O–O bonds needed to form that surface. Given that such bond breakage is unlikely to be favorable, we henceforth do not consider any termination requiring the breakage of the O–O peroxide bonds for the other surfaces.

B. (11$\bar{2}$0) surface

We investigated six terminations for the (11$\bar{2}$0) surface. These terminations are Li(1)-O_2(2)-Li(3), Li(1)-O_2(1)-Li(2)-O_2(2)-Li(3), O_2(1)-Li(2)-O_2(2)-Li(3), Li(2)-O_2(2)-Li(3), O_2(2)-Li(3), and Li(3) termination. These surfaces are labeled by the atoms that remain after removing a selected atom from the five sites shown in Fig. 2(a). There are two stoichiometric terminations on the (11$\bar{2}$0) surface. One stoichiometric termination is Li(1)-O_2(2)-Li(3) termination, which is generated by removing the O_2 from the O_2(1) site and Li from the Li(2) site. The other stoichiometric termination, Li(2)-O_2(2)-Li(3) termination, is generated by removing O_2(1) and Li(1) atoms from the Li(1)-O_2(1)-Li(2)-O_2(2)-Li(3) termination [Fig. 2(a)]. Other terminations are off-stoichiometric. The Li(1)-O_2(1)-Li(2)-O_2(2)-Li(3) termination is shown in Fig. 2(a). The O_2(1)-Li(2)-O_2(2)-Li(3) termination is generated by removing Li(1) from the Li(1)-O_2(1)-Li(2)-O_2(2)-Li(3) termination. Further removing Li(2) from the Li(2)-O_2(2)-Li(3) termination, one will get O_2(2)-Li(3) termination.

FIG. 2. (Color online) (a) The surface unit cell and (b) the relaxed structure of the most stable termination of the (11$\bar{2}$0) surface. Red and green atoms are oxygen and lithium, respectively.
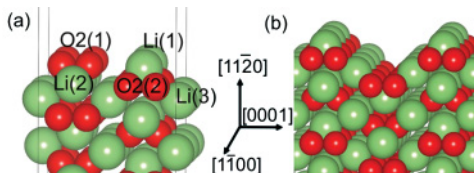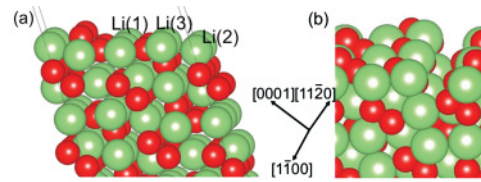

FIG. 3. (Color online) (a) The surface unit cell and (b) the relaxed structure of the most stable termination of the (11$\bar{2}$1) surface. Red and green atoms are oxygen and lithium, respectively.

After removing all Li from Li(1) and Li(2) sites and O_2 from O_2(1) and O_2(2) sites, Li(3) termination is constructed. The most stable termination for the (11$\bar{2}$0) surface is the stoichiometric Li(1)-O_2(2)-Li(3) termination [Fig. 2(b)]. The study by Hummelshøj et al.[20] also predicted the same termination on the (11$\bar{2}$0) surface to be the most stable. The other stoichiometric termination, that is, Li(2)-O_2(2)-Li(3) termination, has considerably higher surface energy (Table II).

C. (11$\bar{2}$1) surface

The (11$\bar{2}$1) surface has not been reported in the literature. The stoichiometric termination is shown in Fig. 3(a). Different surface terminations are generated by removing atoms from different surface sites as labeled in Fig. 3(a). For example, the Li(1)-Li(2)-O, Li(1)-Li(3)-O, and Li(2)-Li(3)-O terminations are constructed by removing Li atoms from Li(3), Li(2), and Li(1) sites, respectively. The other terminations, such as Li(1)-O, Li(2)-O, and Li(3)-O terminations, are generated by removing two Li atoms from the corresponding surface sites. The O termination is generated by removing Li atoms from all three Li sites. We found the Li(1)-Li(3)-O termination [Fig. 3(b)] to be the most stable termination for (11$\bar{2}$1) surface at both the most reducing and the most oxidizing conditions. The stoichiometric termination is not favorable for the (11$\bar{2}$1) surface.

D. (1$\bar{1}$00) surface

There are two Li sites, that is, Li(1) and Li(2), on the (1$\bar{1}$00) surface [Fig. 4(a)]. The stoichiometric termination is shown in Fig. 4(a). The Li(1)-O and Li(2)-O terminations are constructed by removing Li atoms from Li(2) and Li(1) sites, respectively. The O termination is constructed by removing all Li atoms. The stoichiometric termination is not favorable for the (1$\bar{1}$00) surface (Table II). The most stable surface termination is the Li(2)-O termination, as shown in Fig. 4(b). The most stable termination is consistent with the study by Seriani.[37]
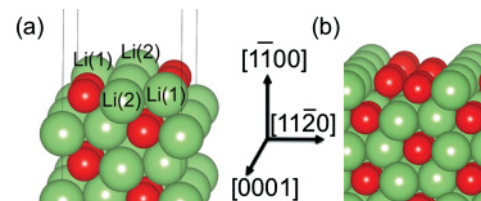

FIG. 4. (Color online) (a) The surface unit cell and (b) the relaxed structure of the most stable termination of surface (1$\bar{1}$00). Red and green atoms are oxygen and lithium, respectively.
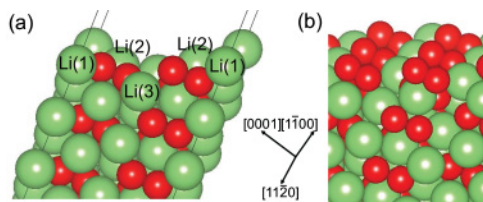
FIG. 5. (Color online) (a) The surface unit cell and (b) the relaxed structure of the most stable termination of the $(1\bar{1}01)$ surface. Red and green atoms are oxygen and lithium, respectively.

E. $(1\bar{1}01)$ surface

The stoichiometric termination is shown in Fig. 5(a). We investigated three Li-deficient terminations, that is, Li(2)-Li(3)-O, Li(1)-Li(3)-O, and Li(3)-O termination. The Li(3)-O termination [Fig. 5(b)] is the most stable termination for the $(1\bar{1}01)$ surface.

F. The Wulff shape of Li_2O_2

The surface energies for the different terminations of low-index surfaces are summarized in Fig. 6 and Table II. The most stable terminations for all low-index surfaces do not change in the range of chemical potentials considered, and the (0001) surface is the lowest energy surface in the Wulff shape. We constructed the Wulff shape for Li_2O_2 based on our calculated surface energies of the most stable terminations in Fig. 6 and Table II in Appendix. Under the most reducing condition (Li-rich and oxygen-poor environment), the Wulff shape is a hexagonal prism with truncated angles [Fig. 7(b)] that is largely composed of the $(11\bar{2}0)$ and (0001) surfaces. Under the most oxidizing condition, the Wulff shape is truncated by the $(11\bar{2}1)$, $(1\bar{1}00)$, and $(1\bar{1}01)$ surfaces. The $(1\bar{1}00)$ surface does not exist in the Wulff shape at the most reducing condition. In the Wulff shape reported in the previous study by Seriani *et al.*,[37] there is an abundant fraction of the $(1\bar{1}00)$ surface, and the $(11\bar{2}0)$ surface is absent. The discrepancy is probably due to the fact that other surfaces, such as $(11\bar{2}0)$, $(11\bar{2}0)$, and $(1\bar{1}01)$ surfaces, were not considered in Seriani's work.
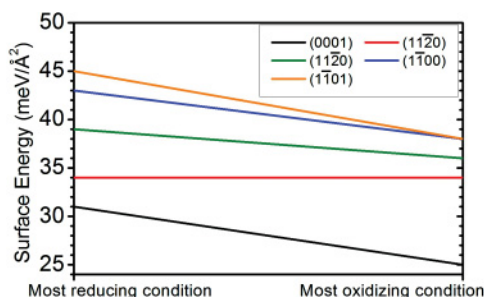

FIG. 6. (Color online) Surface energies for the most stable termination of low-index surfaces of Li_2O_2 from the most reducing condition to the most oxidizing condition. Please refer to the text and Figs. 1–5 for the termination structures. The surface energies for other terminations are provided in Table II.
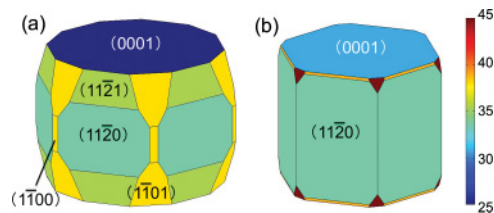

FIG. 7. (Color online) The Wulff shape of Li_2O_2 at (a) the most oxidizing condition and (b) the most reducing condition. The surface energies are shown in the scale bar (in meV/Å^2). The Wulff shape is dominated by the (0001) (top and bottom) and $(11\bar{2}0)$ surfaces (light green).

IV. OXYGEN EVOLUTION REACTION MECHANISM

In this section, we calculate the energy profile and the reaction path of the OER for the (0001), $(11\bar{2}0)$, $(11\bar{2}1)$, $(1\bar{1}00)$, and $(1\bar{1}01)$ surfaces. During charging, the OER in the Li-air battery is essentially the decomposition of Li_2O_2 on the surfaces. Li ions (and electrons e^-) leave the surface under the driving force of the charging potential. At the same time, O_2 molecules are released from the surface. The elementary reaction step of Li desorption and oxygen evolution can be written as follows:

$$Li_xO_y \longrightarrow Li_{x-1}O_y + Li^+ + e^-$$

or

$$Li_xO_y \longrightarrow Li_xO_{y-2} + O_2,$$
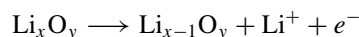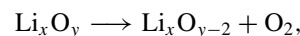
where Li_xO_y denotes the formula of the surface structure. For all surfaces investigated in this study, there are two formulas of Li_2O_2 on the surface of our calculation supercell. Therefore, the initial structure in the surface unit cell can be denoted by the formula Li_4O_4. The value of x or y is decreased by one or two at each reaction step, until both reach zero when the entire OER path is completed. The final termination is identical with the initial one.

Using the slab model described in the Methods section, we calculated the energy of each intermediate reaction step in the OER by removing a Li atom or a O_2 molecule from the surface. The same removal was performed on both the top and the bottom surfaces of the slab to ensure that the surfaces remain identical. The reaction free energy of each of the intermediate steps is given by the following expression:

$$\Delta G = \tfrac{1}{2}\left[E_{\text{slab}}^{\text{step}} - E_{\text{slab}}^0 - \Delta N_O \cdot \mu_O^0 - \Delta N_{Li} \cdot \left(\mu_{Li}^0 - eU\right)\right],$$

(12)

where $E_{\text{slab}}^{\text{step}}$ is the total energy of the slab at the current step, E_{slab}^0 is the total energy of the initial slab, ΔN_O and ΔN_{Li} are the total numbers of removed O and Li atoms, and the factor of 1/2 is to account for the two surfaces of the slab.

The chemical potential of O_2 is defined in the Methods section. The chemical potential of Li, μ_{Li}^0, is set to be the chemical potential of bulk Li metal. The term $-eU$ is added to the chemical potential of Li in Eq. (12) to account for the energy of electron transfer at the applied potential U.
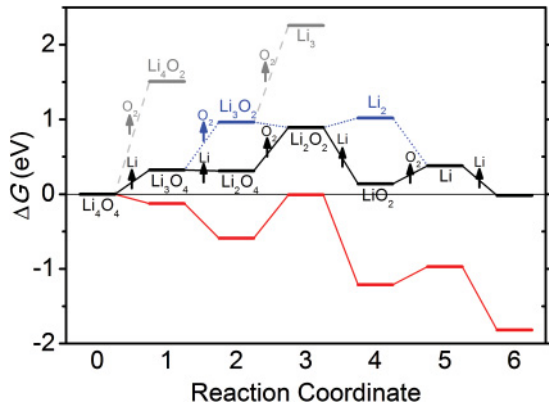
FIG. 8. (Color online) The energy profile for the OER on the (0001) surface, starting from the most stable termination. The lowest energy path at potential $U = 2.82$ V is shown in black. Alternative paths at the same potential are shown in blue and gray. The reaction free energies ΔG of all intermediate steps are negative for the lowest energy path at $U = 3.27$ V (red).

A. OER path for the (0001) surface

The black line in Fig. 8 gives the energy profile of the lowest energy OER path on the (0001) surface at the equilibrium potential $U = 2.82$ V. The predicted OER path is as follows.

(i) Desorption of a Li atom from the surface with an energy barrier of 0.32 eV to form Li_3O_4 at the surface.

(ii) Desorption of another Li from the surface to form a superoxidelike Li_2O_4 structure at the surface. The lowest energy path shows that the formation of superoxide 2 LiO_2 is the first step in the decomposition of Li_2O_2.

(iii) Desorption of an O_2 molecule with an energy barrier of 0.58 eV, thereby recovering the perioxide stoichiometry of Li_2O_2.

(iv) The desorption of the remaining one formula of Li_2O_2 in the surface unit cell is predicted to occur via the desorption of another Li atom, followed by desorption of an O_2 molecule, and finally the desorption of the last Li atom. The energy barrier to evolve the second O_2 is 0.24 eV.

There are alternative paths at some of the reaction steps that lead to slightly higher overall reaction barriers (blue lines in Fig. 8). For example, desorption of O_2 can take place instead of the desorption of a second Li in step 2, with an energy barrier of 0.64 eV. Desorption of O_2 can also take place in step 4 with an energy barrier of 0.48 eV. The other alternative paths (gray lines in Fig. 8) have far higher reaction barriers (>1 eV).

For the lowest energy path, a charge potential of 3.27 V, that is, an overpotential of 0.45 V, would make the energy of all intermediate steps negative. In all cases, the energy barrier for O_2 desorption is positive and is not affected by the applied potential U. The highest energy barrier for O_2 evolution, 0.58 eV, occurs in step 3 and corresponds to the activation energy for the OER process on the (0001) surface.

B. OER path for the (11$\bar{2}$0) surface

The lowest energy OER path for the (11$\bar{2}$0) surface is given by the black line in Fig. 9. The predicted reaction path is as follows.
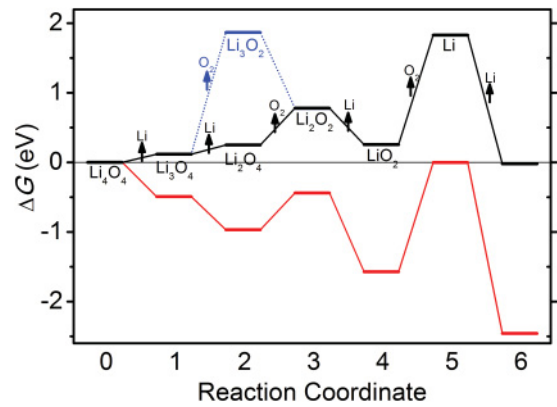

FIG. 9. (Color online) The energy profile for the OER on the (11$\bar{2}$0) surface, starting from the most stable termination. The lowest energy path at potential $U = 2.82$ V is shown in black. Alternative paths at the same potential are shown in blue and gray. The reaction free energies ΔG of all intermediate steps are negative for the lowest energy path at $U = 3.43$ V (red).

(i) Desorption of a Li atom from the Li(1) site followed by the desorption of Li from the Li(3) site [Fig. 2(a)]. The energy barriers for removing these two Li atoms are 0.12 and 0.13 eV, respectively. An alternative path to desorb O_2 at step 2 has a very high energy barrier of 1.75 eV (blue line in Fig. 9). It is therefore more favorable to form the superoxidelike structure Li_2O_4 on the (11$\bar{2}$0) surface in the first two steps.

(ii) The next step (step 3) is to desorb O_2 from site $O_2(2)$ [Fig. 2(a)] with the energy barrier of 0.57 eV, thereby restoring the stoichiometry to Li_2O_2.

(iii) The desorption of the remaining Li_2O_2 is predicted to occur via the removal of a Li atom, followed by the desorption of the second O_2 molecule [from the $O_2(1)$ site as illustrated in Fig. 2] with an energy barrier of 1.57 eV. The final step involves the desorption of the last Li atom.

The high energy barrier for the O_2 evolution suggests a high activation energy for the OER process on the (11$\bar{2}$0) surface. As shown in red in Fig. 9, the energy for all intermediate steps is negative at a charging potential of 3.43 V. The overpotential for OER on the (11$\bar{2}$0) surface is therefore 0.61 V. There is, however, still an activation barrier in the path for O_2 to be released.

C. OER path for the (11$\bar{2}$1) surface

From Fig. 10, we may observe that the first two steps of the lowest energy OER path are the desorption of Li atoms on Li(3) site, followed by the desorption of another Li atom on the Li(1) site [Fig. 3(a)]. The energy barriers for the first two steps are 0.19 and 0.11 eV, respectively. An alternative path where the Li atom on the Li(1) site is first desorbed followed by the Li atom on the Li(3) site has a higher energy barrier of 0.39 V (as shown in the blue line Fig. 10). Oxygen desorption occurs at steps 3 and 6 with energy barriers of 0.35 and -0.06 eV, respectively. All other paths have significantly higher energy than the lowest energy path.

The reaction energy for all intermediate steps are negative under charging potential 3.14 V (red line in Fig. 10), which corresponds to an overpotential of 0.32 V.
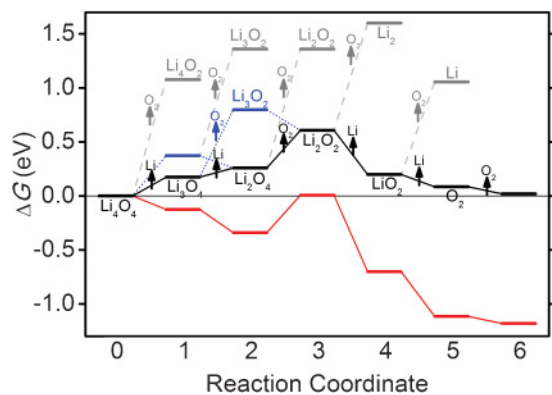
FIG. 10. (Color online) The energy profile for the OER on the $(11\bar{2}1)$ surface, starting from the most stable termination. The lowest energy path at potential $U = 2.82$ V is shown in black. Alternative paths at the same potential are shown in blue and gray. The reaction free energies ΔG of all intermediate steps are negative for the lowest energy path at $U = 3.14$ V (red).

D. OER path for the $(1\bar{1}00)$ surface

Even though there is only a small fraction of $(1\bar{1}00)$ surface in the Wulff shape of Li_2O_2, we also considered the OER energy profile on this surface. The reaction path with lowest energy barrier is given by the black line in Fig. 11. The reaction energy for the desorption of the first Li atom is 0.27 eV. The energy barriers are 0.21 and 0.36 eV for O_2 evolution at steps 3 and 4, respectively. Alternative paths for O_2 evolution at step 1 or step 2 have energy barriers of 1.31 and 0.51 eV, respectively.

A potential of $U = 3.09$ V is required to make the free energy of all intermediate step negative (the red line in Fig. 11). The overpotential is therefore 0.27 V for the OER on the $(1\bar{1}00)$ surface.

E. OER path for the $(1\bar{1}01)$ surface

The reaction path with lowest energy barrier on the $(1\bar{1}01)$ surface is given by the black line in Fig. 12. There is an energy barrier of 0.04 and 0.16 eV for the desorption of Li atoms in
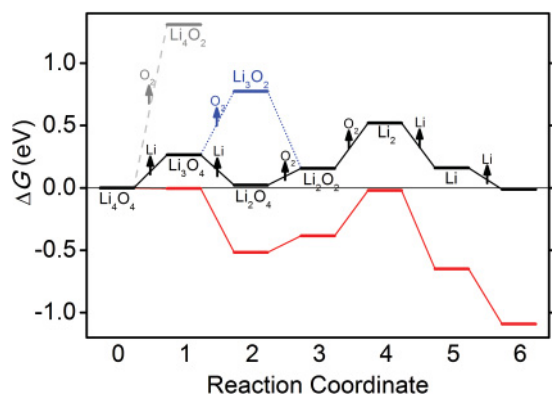

FIG. 11. (Color online) The energy profile for the OER on the $(1\bar{1}00)$ surface, starting from the most stable termination. The lowest energy path at potential $U = 2.82$ V is shown in black. Alternative paths at the same potential are shown in blue and gray. The reaction free energies ΔG of all intermediate steps are negative for the lowest energy path at $U = 3.09$ V (red).
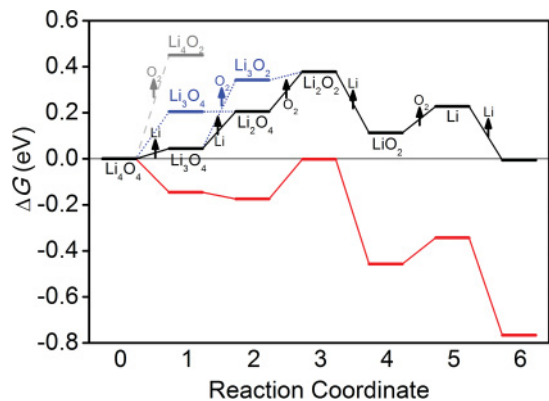

FIG. 12. (Color online) The energy profile for the OER on the $(1\bar{1}01)$ surface, starting from the most stable termination. The lowest energy path at potential $U = 2.82$ V is shown in black. Alternative paths at the same potential are shown in blue and gray. The reaction free energies ΔG of all intermediate steps are negative for the lowest energy path at $U = 3.02$ V (red).

step 1 [Li(3) site in Fig. 5] and step 2 [Li(1) site], respectively. An alternative path to desorb these two Li atoms in the reverse order is shown in the blue line (Fig. 12). Evolution of O_2 occurs at steps 3 and 5 with energy barriers of 0.17 and 0.11 eV, respectively. Alternative paths to desorb O_2 at steps 1 (the gray line in Fig. 12) or 2 (blue line in Fig. 12) have energy barriers of 0.45 and 0.30 eV, respectively.

A potential of $U = 3.02$ V is required to make the free energy of all intermediate steps negative (the red line in Fig. 12), corresponding to an overpotential is 0.20 V for the $(1\bar{1}01)$ surface. The energy barriers for oxygen evolution is lower than for the other surfaces.

V. DISCUSSION

In this work, we identified the most stable termination of the low-index surfaces of Li_2O_2 in the lithium and oxygen chemical potential ranges for which Li_2O_2 is stable. Our results are summarized in Fig. 6 and Table II. The most stable surface terminations tend to be oxygen rich and lithium deficient, except for the $(11\bar{2}0)$ surface, which is stoichiometric. In all cases, the most stable terminations of all surfaces do not change in the range of chemical potential considered. This is not surprising given the limited chemical potential range under which Li_2O_2 is stable. We find that breaking any O–O bonds on the surface comes with a high energy penalty. The fact that the O_2 molecule remains intact on the surface may facilitate the adsorption/desorption of O_2. The Wulff shape—the shape of the particle with lowest surface energy—is dominated by (0001) and $(11\bar{2}0)$ surfaces with only a very small amount of other surfaces [such as $(11\bar{2}1)$, $(1\bar{1}00)$, and $(1\bar{1}01)$ surfaces] present under oxidizing conditions. These surfaces in the Wulff shape become relatively lower in energy with respect to the $(11\bar{2}0)$ surface under oxidizing conditions as these surfaces are oxygen rich while the $(11\bar{2}0)$ surfaces is stoichiometric.

Our calculated reaction paths for oxygen release show that all the surfaces of Li_2O_2 first decompose into a superoxidelike LiO_2 structure via the removal of lithium atoms. This finding is somewhat supported by the experimental findings that lithium

superoxide is an intermediate in the formation of Li_2O_2 in the ORR.[15,18,19]

For all surfaces the desorption of the first Li atom is not energetically favorable at the equilibrium potential at which Li_2O_2 should decompose into Li and O_2. Hence, some overpotential will be required to extract Li from a surface. We find that the energy barrier for Li desorption is 0.13 and 0.32 eV for the $(11\bar{2}0)$ and (0001) surfaces, respectively. The energy barrier for other surfaces is also in this range. This superoxide is the state with the highest oxygen activity along the decomposition path, which explains its strong reactivity toward organic species such as the carbonate electrolyte typically used in Li batteries.[6,11–14]

Oxygen evolution typically takes place following the formation of the superoxidelike surface. The energy barriers we find for the oxygen evolution steps are significantly higher (ranging from 0.17 to 1.57 eV) than those for Li desorption on most surfaces investigated (Table I). In particular, the most abundant surfaces [the (0001) and $(11\bar{2}0)$ surfaces] in the Wulff shapes of Li_2O_2 have the highest energy barrier for oxygen evolution among all the surfaces considered. This is not unexpected as the surfaces with the most strongly bonded O_2 probably derive their low surface energy from that strong binding, while the other surfaces [such as $(11\bar{2}1)$, $(1\bar{1}00)$, and $(1\bar{1}01)$ surfaces], which only make up a small fraction of the Wulff shape, or which are not present at all, have a lower barrier for O_2 release. It is possible that these surfaces are stabilized in solution by the adsorption of solvent species. Any stabilization of the O_2 group on the surface will increase the barrier for O_2 release. Importantly, the barriers to release O_2 from the superoxide are not affected by the applied potential in our approach. Our supercells only have two peroxide units on the surface. While the first O_2 release has a significant barrier on the (0001) surface, the release of the second O_2 is much easier. This is not the case for the $(11\bar{2}0)$ surface. This result may indicate that the step migration mechanism may be more likely on the $(11\bar{2}0)$ surface: Once the first O_2 is removed, moving subsequent O_2 may be easier and may occur as a reaction front sweeping across the surface. Given that the reaction barrier of O_2 release is higher than Li desorption, we expect oxygen evolution to be a rate-limiting step in the OER.

Due to the energy barriers for lithium desorption and oxygen evolution at the equilibrium potential of Li_2O_2 decomposition, an overpotential is required to give negative reaction free energies for all intermediate steps of the OER (red curves in Figs. 8–12). The predicted overpotential for Li desorption ranges from 0.20 to 0.61 V (Table I). Experimentally, charging

voltages as high as 4.0–4.5 V have been observed, corresponding to an overpotential of more than 1 V.[2–4] Recent studies have attributed these high charging voltages to the decomposition of lithium carbonate, which is formed as a result of side reactions with electrolyte during discharging.[6,11–14] The decomposition voltage of lithium carbonate is 4.2 V, which is close to the observed charging voltage in carbonate-based electrolytes. Recent cyclic voltammetry measurements on pure Li_2O_2 have identified an oxidization peak at 3.2–3.6 V for Li_2O_2,[6,12,18,19] which corresponds to a charging overpotential of 0.2–0.6 V compared to the experimental equilibrium potential 2.96 V. Our calculated overpotentials are therefore in reasonable agreement with the measured values.

We can estimate the kinetic rate of Li desorption from the calculated activation energies of the OER process. As an approximation, we assume that the overall activation energy $\Delta G_{activation}$ for a charging step (i.e., the complete stripping of a surface layer) to be given by the highest energy barrier along the lowest energy OER path. We note that this approximation does not take into account other possible sources of rate limitation (e.g., possible electronic conductivity limitations). The activation energy is 0.17, 0.36, 0.35, 0.58, and 1.57 eV on the $(1\bar{1}01)$, $(1\bar{1}00)$, $(11\bar{2}1)$, (0001), and $(11\bar{2}0)$ surfaces, respectively. Given that the rate of Li desorption corresponds to the current density on the cathode surface, we may estimate the surface current density using an Arrhenius relation as follows:[38]

$$i = 2e \frac{N_{site}}{A} k_0 e^{-\Delta G_{activation}/kT},$$

where N_{site}/A is the number of O_2 sites per surface area, k_0 is the prefactor, and the factor of two corresponds to two electrons (two Li ions) per O_2. There are no experimental measurements of the prefactor in the electrochemical decomposition of Li_2O_2. However, experimental studies of the thermal desorption of Li_2O_2 measured a prefactor of 10^{14}–10^{16} s^{-1} (Ref. 39). Assuming a prefactor $k = 10^{15}$ s^{-1}, we were able to estimate the current density on each surface of Li_2O_2, as summarized in Table I. The current density is not dependent on the overpotential as the activation barrier is given by the oxygen evolution, which is voltage independent. The current density is estimated in the range of 10^7–10^{10} $\mu A/cm^2$ on the $(11\bar{2}1)$, $(1\bar{1}01)$, and $(1\bar{1}00)$ surfaces. However, the fraction of the $(1\bar{1}01)$, $(11\bar{2}1)$, and $(1\bar{1}00)$ surfaces in the Wulff shape of Li_2O_2 is small under the most oxidizing condition and negligible under the most reducing condition. The current density is relatively lower on the (0001) surface ($\sim 10^2$ $\mu A/cm^2$)

TABLE I. Overpotential and reaction energy barrier of the OER on the low-index surfaces of Li_2O_2.

Surface orientation	(0001)	$(11\bar{2}0)$	$(11\bar{2}1)$	$(1\bar{1}00)$	$(1\bar{1}01)$
Energy barrier for Li desorption (eV)[a]	0.32	0.13	0.19	0.27	0.16
Acvitation energy for O_2 desorption (eV)[b]	0.58	1.57	0.35	0.36	0.17
Overpotential (V)[c]	0.45	0.61	0.32	0.27	0.20
Estimated surface current density ($\mu A/cm^2$)[d]	10^2	10^{-14}	$<10^7$	$<10^7$	$<10^{10}$

[a]The maximum energy barrier for Li desorption at $U = 2.82$ V.
[b]The maximum energy barrier for the entire reaction path of OER.
[c]The free energy of all intermediate steps is negative at the overpotential referring to $U_0 = 2.82$ V.
[d]Exchange current density per surface area of Li_2O_2 estimated using prefactor $k_0 = 10^{15}$ s^{-1}.

and is negligible on the ($11\bar{2}0$) surface ($\sim 10^{-14}$ μA/cm^2). These two surfaces are dominant in the Wulff shape of Li$_2$O$_2$.

Previous experimental work has estimated that the power density per cathode area in a Li-air battery is around 0.1 mA/cm^2, which corresponds to a current density of 0.2 μA/cm^2 per unit surface area of porous carbon.[15] Since it is not clear what the percentage of the porous carbon surface is covered by Li$_2$O$_2$, it is difficult to estimate the current density per surface area of Li$_2$O$_2$. The upper limit of cathode current density can be estimated by assuming 100% coverage of a certain Li$_2$O$_2$ surface on porous carbon and assuming that all these surfaces of Li$_2$O$_2$ are active in reaction. To benchmark the reaction rate on the Li$_2$O$_2$ surfaces, we found the upper limit of cathode current density to be 10 mA/cm^2 and 10^{-15} mA/cm^2 for the (0001) and ($11\bar{2}0$) surfaces, respectively. Given that a cell current density of more than 100 mA/cm^2 in discharging is desirable for electric vehicle applications,[17] a similar charging rate would also be desirable to realize the fast recharging of batteries for electric vehicles. The current density on the dominant surfaces of Li$_2$O$_2$ during charging is significant lower than the desirable value. Therefore, the kinetics for the OER is slow on the abundant Li$_2$O$_2$ surfaces. Our work provides some evidence that the poor kinetics for the OER is the probable cause of the low charging rate of Li-air cells.

It is worth noting that our surface calculations are performed in vacuum and that the surface energies and the Wulff shape may change in the presence of solvent and electrolyte. Given that (0001) and ($11\bar{2}0$) surfaces are much more stable compared to other surfaces, a small change in the surface energy will not change the trend observed in our calculations.

VI. CONCLUSION

Using first-principles calculations, we identified the surface structures and their energies of multiple low-index surfaces of Li$_2$O$_2$. We find that (0001) and ($11\bar{2}1$) surfaces dominate the Wulff shape of Li$_2$O$_2$. In all the surfaces investigated, we found that decomposition starts with Li removal to form a superoxide and that oxygen evolution has the highest energy barrier along the decomposition path. Our first principle calculations have shown that the kinetic rate of OER is highly dependent on surface orientation. The kinetics of OER is slow on the abundant surfaces, such as the ($11\bar{2}0$) and (0001) surfaces, but is faster on the higher energy surfaces. The low charging rate and high overpotential of the Li-air batteries is probably caused by the poor kinetics for the OER.

ACKNOWLEDGMENTS

APPENDIX: SURFACE ENERGIES FOR ALL SURFACE TERMINATIONS

TABLE II. Surface energies for different terminations of low-index surfaces of Li$_2$O$_2$ under the most reducing and most oxidizing conditions (in meV/Å^2). Please refer to Sec. II for the range of chemical potentials and refer to Sec. III for the surface termination structures.

Orientation	Terminations	Li$_2$O limit	O$_2$ gas limit	Li metal limit
(0001)	O(1)-Li(1)-O(2)-Li(2)	31	25	187
	Li(1)-O(2)-Li(2)	78	84	−78
	Li(2)	62	68	−94
	O(2)-Li(2)	107	101	263
($11\bar{2}0$)	Li(1)-O$_2$(2)-Li(3)	34	34	34
	Li(1)-O$_2$(1)-Li(2)-O$_2$(2)-Li(3)	49	45	161
	O$_2$(1)-Li(2)-O$_2$(2)-Li(3)	60	51	283
	Li(2)-O$_2$(2)-Li(3)	103	103	103
	O$_2$(2)-Li(3)	41	37	153
	Li(3)	106	110	−5
($11\bar{2}1$)	Stoichiometric	52	52	52
	Li(1)-Li(2)-O	50	46	141
	Li(1)-Li(3)-O	39	36	130
	Li(2)-Li(3)-O	59	56	150
	Li(1)-O	45	38	226
	Li(2)-O	58	51	239
	Li(3)-O	52	45	233
	O	52	42	324
($1\bar{1}00$)	Stoichiometric	51	51	51
	Li(2)-O	43	38	172
	Li(1)-O	48	43	176
	O	48	39	305
($1\bar{1}01$)	Stoichiometric	56	56	56
	Li(2)-Li(3)-O	51	49	111
	Li(1)-Li(3)-O	49	44	168
	Li(3)-O	45	38	223

*gceder@mit.edu

[1] K. M. Abraham and Z. Jiang, J. Electrochem. Soc. **143**, 1 (1996).

[2] T. Ogasawara, A. Débart, M. Holzapfel, P. Novák, and P. G. Bruce, J. Am. Chem. Soc. **128**, 1390 (2006).

[3] A. Débart, J. Bao, G. Armstrong, and P. G. Bruce, J. Power Sources **174**, 1177 (2007).

[4] A. Débart, A. J. Paterson, J. Bao, and P. G. Bruce, Angew. Chem. Int. Ed. **47**, 4521 (2008).

[5] A. K. Thapa and T. Ishihara, J. Power Sources **196**, 7016 (2011).

[6] A. K. Thapa, K. Saimen, and T. Ishihara, Electrochem. Solid State Lett. **13**, A165 (2010).

[7] R. R. Mitchell, B. M. Gallant, C. V. Thompson, and Y. Shao-Horn, Energy Environ. Sci. **4**, 2952 (2011).

[8] A. Dobley, J. Dicarlo, and K. M. Abraham, in *Proceedings of the 41st Power Sources Conference* (National Technical Information Service, Philadelphia, PA, 2004).

[9] Y.-C. Lu, Z. Xu, H. A. Gasteiger, S. Chen, K. Hamad-Schifferli, and Y. Shao-Horn, J. Am. Chem. Soc. **132**, 12170 (2010).

[10] Y.-C. Lu, H. A. Gasteiger, M. C. Parent, V. Chiloyan, and Y. Shao-Horn, Electrochem. Solid-State Lett. **13**, A69 (2010).

[11] F. Mizuno, S. Nakanishi, Y. Kotani, S. Yokoishi, and H. Iba, Electrochemistry **78**, 403 (2010).

[12] B. D. Mccloskey, D. S. Bethune, R. M. Shelby, G. Girishkumar, and A. C. Luntz, J. Phys. Chem. Lett. **2**, 1161 (2011).

[13] S. a. Freunberger, Y. Chen, Z. Peng, J. M. Griffin, L. J. Hardwick, F. BardeÌ, P. NovaÌk, and P. G. Bruce, J. Am. Chem. Soc. **133**, 8040 (2011).

[14] J. Xiao, J. Hu, D. Wang, D. Hu, W. Xu, G. L. Graff, Z. Nie, J. Liu, and J.-G. Zhang, J. Power Sources **196**, 5674 (2011).

[15] Y.-C. Lu, H. A. Gasteiger, E. Crumlin, R. McGuire, and Y. Shao-Horn, J. Electrochem. Soc. **157**, A1016 (2010).

[16] Y.-C. Lu, D. G. Kwabi, K. P. C. Yao, J. R. Harding, J. Zhou, L. Zuin, and Y. Shao-Horn, Energy Environ. Sci. **4**, 2999 (2011).

[17] G. Girishkumar, B. McCloskey, A. C. Luntz, S. Swanson, and W. Wilcke, J. Phys. Chem. Lett. **1**, 2193 (2010).

[18] C. O. Laoire, S. Mukerjee, K. M. Abraham, E. J. Plichta, and M. A. Hendrickson, J. Phys. Chem. C **113**, 20127 (2009).

[19] C. O. Laoire, S. Mukerjee, K. M. Abraham, E. J. Plichta, and M. A. Hendrickson, J. Phys. Chem. C **114**, 9178 (2010).

[20] J. S. Hummelshøj, J. Blomqvist, S. Datta, T. Vegge, J. Rossmeisl, K. S. Thygesen, A. C. Luntz, K. W. Jacobsen, and J. K. Nørskov, J. Chem. Phys. **132**, 071101 (2010).

[21] Y. Xu and W. A. Shelton, J. Chem. Phys. **133**, 024703 (2010).

[22] G. Kresse and J. Furthmüller, Phys. Rev. B **54**, 11169 (1996).

[23] P. E. Blöchl, Phys. Rev. B **50**, 17953 (1994).

[24] M. Ramamoorthy, D. Vanderbilt, and R. D. King-Smith, Phys. Rev. B **49**, 16721 (1994).

[25] A. Christensen and E. A. Carter, Phys. Rev. B **58**, 8050 (1998).

[26] X.-G. Wang, A. Chaka, and M. Scheffler, Phys. Rev. Lett. **84**, 3650 (2000).

[27] K. Reuter and M. Scheffler, Phys. Rev. B **65**, 035406 (2001).

[28] K. Reuter and M. Scheffler, Phys. Rev. Lett. **90**, 046103 (2003).

[29] L. Wang, F. Zhou, Y. S. Meng, and G. Ceder, Phys. Rev. B **76**, 165435 (2007).

[30] L. Wang, F. Zhou, and G. Ceder, Electrochem. Solid-State Lett. **11**, A94 (2008).

[31] D. Kramer and G. Ceder, Chem. Mater. **21**, 3799 (2009).

[32] K. Reuter and M. Scheffler, Phys. Rev. B **68**, 045407 (2003).

[33] A. F. Kohan, G. Ceder, D. Morgan, and Chris G. Van de Walle, Phys. Rev. B **61**, 15019 (2000).

[34] J. X. Zheng, G. Ceder, T. Maxisch, W. K. Chim, and W. K. Choi, Phys. Rev. B **73**, 104101 (2006).

[35] J. X. Zheng, G. Ceder, T. Maxisch, W. K. Chim, and W. K. Choi, Phys. Rev. B **75**, 104112 (2007).

[36] L. Wang, T. Maxisch, and G. Ceder, Phys. Rev. B **73**, 195107 (2006).

[37] N. Seriani, Nanotechnology **20**, 445703 (2009).

[38] J. K. Nørskov, J. Rossmeisl, A. Logadottir, L. Lindqvist, J. R. Kitchin, T. Bligaard, and H. Jónsson, J. Phys. Chem. B **108**, 17886 (2004).

[39] T. Tanifuji and S. Nasu, J. Nucl. Mater. **87**, 189 (1979).